Title

Unusual C–H Bond Activation and C(sp3)–C(sp3) Bond Formation at an Fe(II) Bis(amide) Carbene Complex

Journal

Organometallics, 39(1)

ISSN

0276-7333

Authors

Wong, Anthony
Guevara, Kevin
Wu, Guang
et al.

Publication Date

2020-01-13

DOI

10.1021/acs.organomet.9b00674

Peer reviewed

ORGANOMETALLICS

Article

pubs.acs.org/Organometallics

Unusual C−H Bond Activation and C(sp^3)−C(sp^3) Bond Formation at an Fe(II) Bis(amide) Carbene Complex

Anthony Wong, Kevin Guevara, Guang Wu, and Gabriel Ménard*

Department of Chemistry and Biochemistry, University of California, Santa Barbara, California 93106, United States

Supporting Information

ABSTRACT: Treatment of (IMes)Fe(NTMS$_2$)$_2$ with 4 equiv of methanesulfonyl chloride (MsCl = MeSO$_2$Cl) resulted in a complex reaction sequence involving substitution of two TMS groups for Ms, followed by the unexpected C(sp^3)−H bond activation of Ms and subsequent C(sp^3)−C(sp^3) bond formation to generate the bimetallic Fe complex, [IMesH]$_2$[Cl$_2$Fe(N(TMS)SO$_2$(CH$_2$)$_2$SO$_2$N(TMS))$_2$FeCl$_2$] (**1**) (IMes = 1,3-bis(2,4,6-trimethylphenyl)-imidazole-2-ylidene; TMS = SiMe$_3$). Extending this C−H activation/C−C bond-forming chemistry to larger alkylsulfonyl chloride chains (i.e., Et and Bu) similarly resulted in C−C coupling, but with decreased chemoselectivity. Detailed mechanistic studies, including using possible intermediate model compounds, were performed in order to elucidate a unifying mechanism for this previously unknown avenue to C(sp^3)−C(sp^3) bond formation.

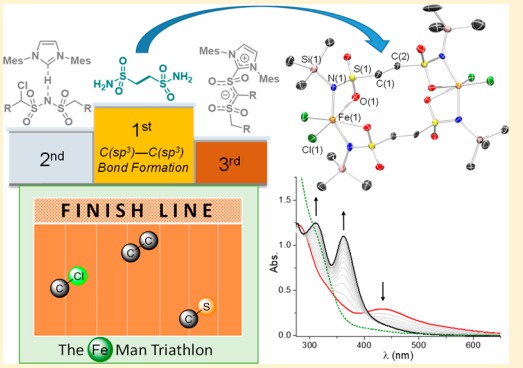

C−H bond activation is an attractive avenue for the transformation of inexpensive and abundant feedstocks into value-added commodity chemicals. At the industrial level, for example, the DuPont "butox" process catalyzes the partial oxidation of *n*-butane to maleic anhydride via a heterogeneous vanadium phosphorus oxide (VPO) catalyst.[1−3] While most research assigned the vanadyl (V=O) centers as the reactive sites for butane C−H bond activation, recent DFT studies suggest that the catalyst support P=O bonds, tethered to neighboring vanadyls, may instead be responsible, reacting by a cooperative proton-coupled electron transfer (PCET) mechanism with neighboring high-valent V centers (Scheme 1a).[4−6] In order to probe this possible new main-group mediated C−H bond functionalization chemistry, we have recently reported a suite of molecular mono- or multimetallic VPO model complexes of the general formula, (R$_x$V^n−L)$_y$P(O)Ar$_{(3-y)}$ (R$_x$ = Cp$_2$, *n* = +3, L = O, *y* = 1, 2, and 3, Ar = Ph; R$_x$ = Cp$_2$, *n* = +3, L = O(O)C(C$_6$H$_4$), *y* = 1 and 3, Ar = Ph; R$_x$ = (Ph$_2$N)$_3$, *n* = +5, L = N, *y* = 1, Ar = Ph, C$_6$F$_5$) (Cp = η^5-C$_5$H$_5$).[7−10] All of these molecules bear a central M−L−E=O framework where M is the metal redox reservoir (e.g., V), L is a resonance linker atom (e.g., O and N) or fragment (e.g., aryl), and E is the main group center (e.g., P). Using the high-valent (Ph$_2$N)$_3$V=N−P(O)Ar$_2$ (Ar = Ph or C$_6$F$_5$) complexes, we found convincing evidence supporting this proposed PCET pathway using an H atom donor, as well as an H atom surrogate in the form of a TMS$^\bullet$ donor (TMS = Me$_3$Si) (Scheme 1a).[10] In this report, we outline our attempted expansion into new M−L−E=O frameworks, in particular containing M = Fe and E = S. What we unexpectedly discovered was a reaction sequence involving the spontaneous C(sp^3)−H bond activation and C(sp^3)−C(sp^3) bond formation chemistry outlined in Scheme 1b. Detailed mechanistic studies were performed in an attempt to

Scheme 1. DFT/Experimental Reports and C−H Bond Activation and C−C Bond Formation[a]

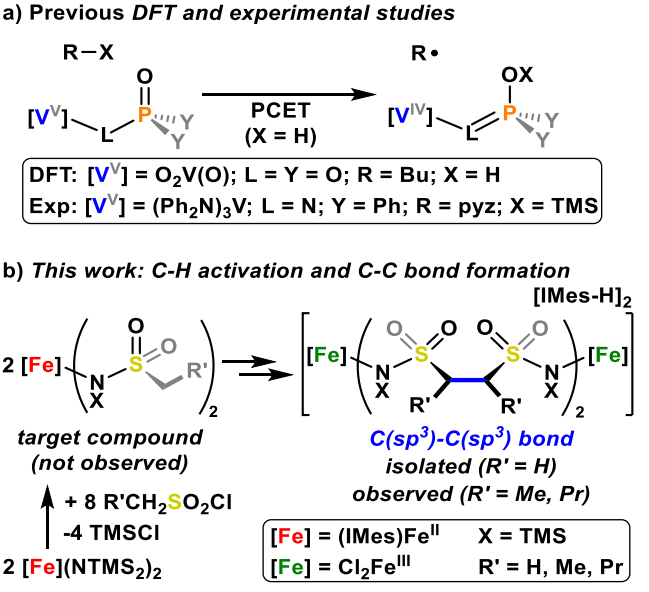

[a](a) Previous DFT/experimental reports on main-group mediated C−H functionalization (pyz = pyrazine; TMS = SiMe$_3$). (b) C−H bond activation and C−C bond formation using an Fe(II) bis(amide) carbene complex.

Received: October 11, 2019

DOI: 10.1021/acs.organomet.9b00674
Organometallics XXXX, XXX, XXX−XXX

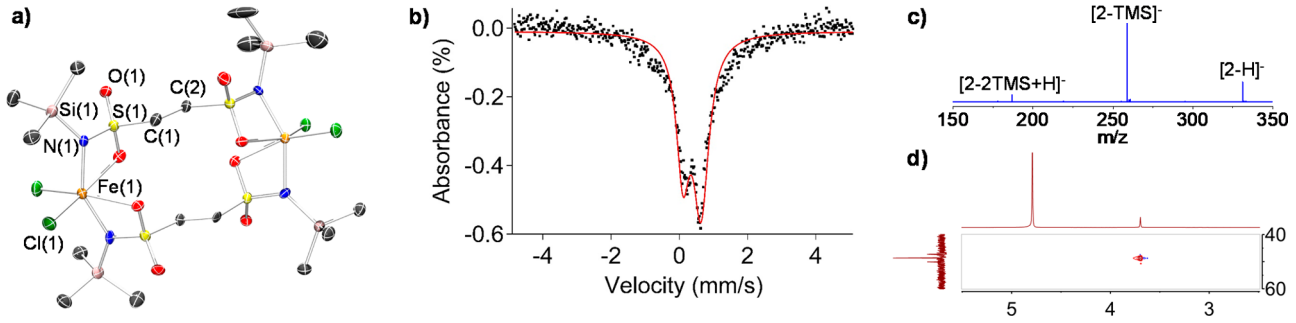

Figure 1. (a) Solid-state molecular structure of **1** revealing C(sp^3)−C(sp^3) bond formation (two $[IMesH]^+$, hydrogen atoms, and all solvent molecules are omitted for clarity). (b) Zero-field ^{57}Fe Mössbauer spectrum (90 K) of **1** showing a single quadrupole doublet with an isomer shift (δ) value of 0.37 mm/s and a quadrupole splitting ($|\Delta E_Q|$) value of 0.53 mm/s. (c) Protonolysis of **1** in MeOH and analysis by negative-ion mode ESI-MS showing the C−C coupled fragment **2** in its deprotonated ($[\mathbf{2}\text{-H}]^-$) and desilylated derivatives ($[\mathbf{2}\text{-TMS}]^-$ and $[\mathbf{2}\text{-2TMS} + \text{H}]^-$). (d) Partial ^{1}H−^{13}C HSQC NMR spectrum of **3a** in D_2O highlighting the CH_2−CH_2 fragment.

probe this unusual reaction mechanism involving this previously unknown and potentially new avenue to C(sp^3)−C(sp^3) bond formation.

RESULTS AND DISCUSSION

In attempting to synthesize our target compound (Scheme 1b), we began by treating the previously reported compound, (IMes)Fe($NTMS_2$)$_2$ (IMes = 1,3-bis(2,4,6-trimethylphenyl)-imidazole-2-ylidene),[11] with 4 equiv of methanesulfonyl chloride (MsCl = $MeSO_2Cl$). We originally envisioned that TMSCl elimination would furnish our target compound. Mixing these reagents in toluene at room temperature led to darkening of the red solution and subsequent precipitation of a yellow powder after 3 h of stirring. Isolation of the yellow powder and slow crystallization by diffusion of toluene into a saturated dichloromethane (DCM) solution of the product yielded bright-yellow single crystals suitable for X-ray diffraction (XRD) studies. The solid-state molecular structure confirmed the composition as the new C(sp^3)−C(sp^3) coupled product, $[IMesH]_2[Cl_2Fe(N(TMS)SO_2(CH_2)_2SO_2N(TMS))_2FeCl_2]$ (**1**) (Scheme 1b (R′ = H); Figure 1a). The complex featured standard bond metrics, including a C(1)−C(2) bond length of 1.516(9) Å consistent with a C−C single bond.[12] The local geometry around each Fe is distorted octahedral with ligand contributions from two chloride anions and two sulfonamides adopting a κ^2 binding mode through the N and an O atom. Spectroscopic analysis of **1** by zero-field ^{57}Fe Mössbauer spectroscopy (90 K) revealed the presence of a single Fe-containing species with a quadrupole doublet bearing an isomer shift (δ) value of 0.37 mm/s and a quadrupole splitting ($|\Delta E_Q|$) value of 0.53 mm/s (Figure 1b). The low isomer shift and narrow quadrupole splitting values are consistent with pseudo-octahedral, high-spin Fe^{III} complex **1**.[13] The paramagnetic nature of **1** is further evidenced by a set of four broadened, paramagnetically shifted resonances in the ^{1}H NMR spectrum (Figure S16). Analysis of **1** by UV−vis spectroscopy revealed two absorptions centered at 316 nm (ε = 1.1 × 10^4 M^{-1} cm^{-1}) and 362 nm (ε = 1.0 × 10^4 M^{-1} cm^{-1}) which we assign as ligand-to-metal charge transfer (LMCT) bands on the basis of their high extinction coefficients (ε) (Figure S7).

We next probed if the organic C−C coupled fragment could be extracted from Fe in **1**. We observed clean protonolysis of the Fe−N bonds in **1** upon dissolving it in MeOH. Analysis of the MeOH solution by electron-spray ionization mass spectrometry (ESI-MS) in negative-ion mode revealed major peaks for the free ligand, $(TMS)NHSO_2(CH_2)_2SO_2NH(TMS)$ (**2**) in its deprotonated form $(\mathbf{2}\text{-H})^-$, as well as some of its desilylated derivatives, $[\mathbf{2}\text{-TMS}]^-$ and $[\mathbf{2}\text{-2TMS} + \text{H}]^-$ (Figure 1c). Isolation of the fully desilylated bis(sulfonamide) product $H_2NSO_2(CH_2)_2SO_2NH_2$ (**3a**; Scheme 2) was accomplished by addition of 8 equiv of HCl (2.0 M in Et_2O) to a solution of **1** in acetonitrile, followed by isolation of the solid precipitate. Analysis of this product by ESI-MS revealed the conversion to **3a** (Figure S39). Furthermore, the ^{1}H NMR spectrum of the residue in D_2O confirmed the formation of a single product with a singlet at 3.70 ppm correlating to a triplet in the ^{13}C NMR spectrum at 48.7 ppm as confirmed by 2D ^{1}H−^{13}C HSQC experiments (Figure 1d). Finally, colorless crystals of **3a** were grown by slow evaporation of an aqueous solution of the precipitate and unambiguously revealed the intact C−C linkage with C(1)−C(2) bond metrics identical to those of **1**. Together, these experiments demonstrate the clean formation of a C(sp^3)−C(sp^3) coupled fragment as the major product (~90%).

Scheme 2. Competing C−C (3a−c), C−Cl (4a−c), and C−S (5a−c) Bond-Forming Reactions Using Different Alkylsulfonyl Chlorides and Following Workup

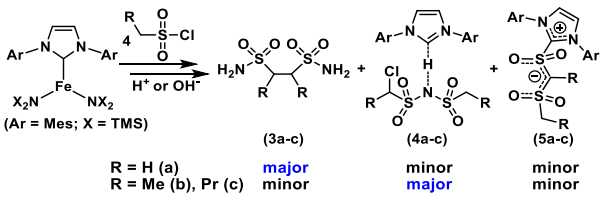

We next probed if this C−H activation/C−C bond-forming chemistry could be extended to longer chains, such as ethyl and butyl. First, treatment of the starting material, (IMes)Fe($NTMS_2$)$_2$, to 4 equiv of ethylsulfonyl chloride (EsCl) in toluene, analogous to the synthesis of **1**, again led to darkening of the red solution, as well as the subsequent formation of an oil. Multiple attempts to obtain single crystals suitable for XRD experiments failed; however, analysis of the crude product by zero-field ^{57}Fe Mössbauer spectroscopy (90 K) revealed the presence of a single monopole with δ and $|\Delta E_Q|$ values of 0.32 and 0.00 mm/s, respectively, suggesting the presence of a highly symmetric Fe^{III} species dissimilar to **1** (Figure S6). Furthermore, analysis of this crude reaction mixture by positive

DOI: 10.1021/acs.organomet.9b00674
Organometallics XXXX, XXX, XXX−XXX

and negative-ion mode ESI-MS again revealed the formation of the C(sp^3)−C(sp^3) coupled product, **3b**; however, this was in addition to two new, more prominent peaks (Figures S47 and S51). Using an acidic workup like the one used in the MsCl reaction resulted in only the iron-containing species, [$FeCl_4$]-[IMesH], being isolated. In order to further characterize the product(s) formed, the crude mixture was instead treated to a basic aqueous solution (NaOH) in air in order to hydrolyze the organic fragments and precipitate the iron oxides (rust). These two new products were selectively isolated, yet we were initially unable to interpret their ^{1}H NMR spectra. Fortunately, both were unambiguously identified by single-crystal XRD studies as the products, **4b** and **5b** (Scheme 2; Figures S32 and S33). Compound **4b** appears to be the result of a double substitution of both TMS groups at N with two EsCl, in addition to a C−Cl bond formation α to the S center. In contrast, we believe **5b** is the product of a side reaction involving a proposed sulfene intermediate (*vide infra*). The ratio of **4b**/**5b** was approximately 2.5:1 based on ^{1}H NMR integration (Figure S17). The proposed formation of all of these compounds will be described in the mechanistic section below. Together, however, we estimate a total yield of approximately 60% for **4b** and **5b** combined based on NMR assignments and integrations (Figure S17), and trace amounts of **3b** based on ESI-MS (Figure S49). Similar products and distributions were obtained with the use of butylsulfonyl chloride to produce the corresponding products, **3c**−**5c** (Scheme 2). In contrast to **3b** and **3c**, we reiterate the yield of **3a** was much higher (~90%), likely suggesting an important steric contribution to the fate of these reactions. Lastly, we note that analogous compounds **4a** and **5a** (Scheme 2) were observed only by ESI-MS and were not isolated.

In order to gain a better mechanistic picture, we focused on the MsCl reaction and synthesized a series of complexes (**6**−**8**) which we initially hypothesized may be relevant to the reaction mechanism (Scheme 3). Compound **6** can be seen as either an Fe^{III} variant of the starting material, (IMes)Fe($NTMS_2$)$_2$, or as a half-fragment of **1** lacking the Ms appendages. The compound was synthesized by addition of [IMesH][Cl] to the known Fe^{III} precursor, Fe($NTMS_2$)$_2$Cl(THF),[14] in benzene. Upon purification, a brick-red powder was isolated in 87% yield. Single-crystals suitable for XRD studies were grown by vapor diffusion of pentane into a saturated benzene solution of **6** and revealed the expected structure, with the anionic portion isostructural to a previous report (Figure S34).[14] The zero-field ^{57}Fe Mössbauer spectrum of **6** (Figure S1) revealed a broad quadrupole doublet with δ and $|\Delta E_Q|$ values of 0.35 and 1.16 mm/s. The UV−vis spectrum of **6** revealed a prominent band at 420 nm (Figure S8), similar to that of the starting material Fe($NTMS_2$)$_2$Cl(THF)[14] at 433 nm, which will be relevant to the mechanistic study below. All other spectroscopic data for **6** are as expected.

Scheme 3. C−C Bond-Forming Reaction (top) and Model Complexes 6−8 for Mechanistic Studies (bottom)

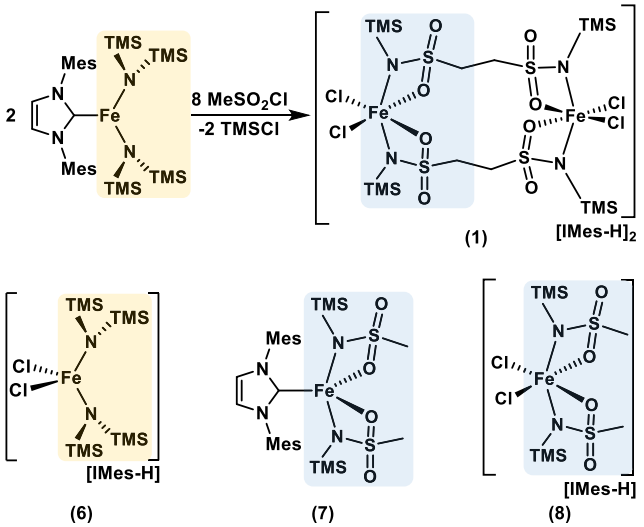

Our original target species, compound **7** (Scheme 1b (R′ = H) and Scheme 3), was next synthesized in a two-step, one-pot protocol involving the addition of Fe($NTMS_2$)$_2$ to 2 equiv of *N*-(trimethylsilyl)methanesulfonamide (MsNH(TMS))[15] resulting in the deprotonation of MsNH(TMS) and formation of TMS_2NH. Next, 1 equiv of IMes was subsequently added directly to this reaction mixture. Following isolation and purification, the product was analyzed by zero-field ^{57}Fe Mössbauer spectroscopy (90 K) and revealed the presence of a quadrupole doublet with δ and $|\Delta E_Q|$ values of 0.55 and 0.97 mm/s, respectively (Figure S2). Single crystals suitable for XRD studies were grown out of a saturated ether solution at −38 °C. The complex displays distorted trigonal bipyramidal symmetry around Fe (Figure S35). The UV−vis spectrum of **7** features a broad absorbance at 298 nm (ε = 7.5 × 10^2 M^{-1} cm^{-1}) (Figure S9).

The last model compound synthesized (**8**, Scheme 3), represents the "half-piece" of **1** and was obtained by an acid−base approach similar to the synthesis of **7**. First, 2 equiv of MsNH(TMS) were added to Fe($NTMS_2$)$_2$Cl(THF) in benzene.[14] Subsequent addition of [IMesH][Cl] and isolation/purification of the product afforded **8** in 89% isolated yield. Single crystals suitable for XRD studies were grown by layering hexamethyldisiloxane (HMDSO) to a saturated THF solution of **8** (Figure 2).

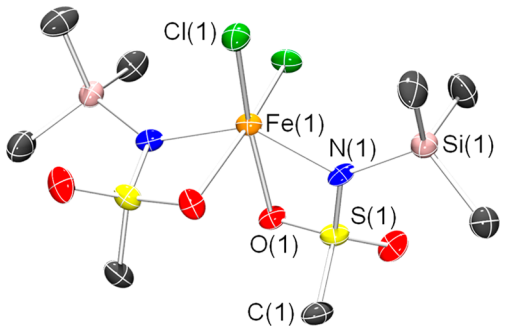

Figure 2. Solid-state molecular structure of **8** representing the "half-fragment" of **1** with identical Fe environments ([IMesH]$^+$ and all hydrogen atoms are omitted for clarity).

Interestingly, all relevant bond metrics and angles in **8** are nearly identical to those in **1** (Table S1). We note that **8** and **1** crystallize in separate space groups, *Pbca* and $P\bar{1}$, respectively, and that **1** does not lie on a center of symmetry and is thus not a product of crystallographic symmetry. The identical Fe environments in **8** and **1** were further confirmed spectroscopically. First, the zero-field ^{57}Fe Mössbauer spectrum of **8** (Figure S3) revealed a single quadrupole doublet with δ and $|\Delta E_Q|$ values of 0.35 and 0.50 mm/s, respectively, virtually

DOI: 10.1021/acs.organomet.9b00674
Organometallics XXXX, XXX, XXX−XXX

identical to the doublet assigned to **1** (0.37 and 0.53 mm/s, respectively; Figure 1b). Second, the UV−vis spectrum of **8** revealed LMCT bands at 316 and 362 nm, identical to those of **1**, but with ε values half as intense, consistent with the reduced metal nuclearity in **8** (Figure S10). Last, protonolysis of **8** with MeOH and subsequent analysis by ESI-MS in negative-ion mode revealed a prominent peak at m/z = 166.04, consistent with the ligand fragment $[MsN(TMS)]^-$ (Figure S41). No $C(sp^3)-C(sp^3)$ products, such as in the protonolysis of **1** (Figure 1c), were observed here.

With model compounds **6**−**8** in hand, we next attempted to establish a unifying mechanism for the C−H activation/C−C bond-forming chemistry (**3**) which would incorporate competing pathways to generate compounds **4** and **5** (Scheme 2). A series of control reactions were first performed. The first involved the reaction of IMes with MsCl in the absence of $Fe(NTMS_2)_2$. Clean conversion to the [IMes][Cl] salt was observed by ^{1}H NMR spectroscopy (Figure S29). The formation of the known cyclic, 4-membered sulfene dimer compound, $(-S(O)_2CH_2-)_2$, is proposed but was not observed spectroscopically.[16] A second control experiment was performed to determine whether IMes was needed in this chemistry. First, 2 equiv of MsCl was slowly added to a toluene solution of $Fe(NTMS_2)_2$ in the absence of IMes. A dark red product was isolated, purified, and crystallized by slow-cooling a saturated HMDSO solution. The solid-state structure revealed the formation of a bridging, bimetallic, all-ferric siloxide complex of the formula, $((TMS_2N)ClFe)_2(\mu\text{-}OTMS)_2$ (**9**) (Scheme 4, Figure S36), analogous in many respects to a

Scheme 4. Reaction of $Fe(NTMS_2)_2$ with MsCl (2 equiv) to Produce 9

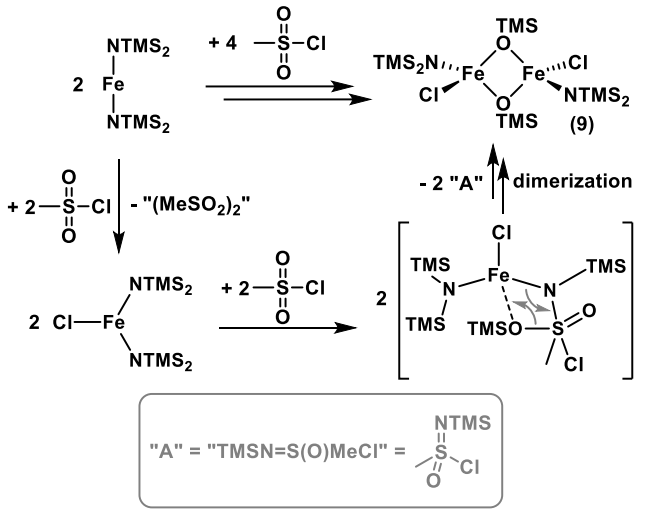

structure obtained by Holland and co-workers involving the reaction of $XFe(NTMS_2)$ with CO_2 to produce $(XFe)_2(\mu\text{-}OTMS)_2$ and the isocyanate, TMSN═C═O (X = formazanate(1−) ligand).[17] Following an analogous mechanism to theirs, we propose that O extrusion from MsCl leads to siloxide formation and production of the unstable *N*-silylmethylsulfonimidoyl chloride (TMSN═S(O)MeCl) byproduct.[18] Two important observations can be made from this control reaction: (1) One of the four equivalents of MsCl oxidatively delivers chlorine to Fe. (2) IMes clearly has an important impact on the reaction outcome (*vide infra*).

We next turned to UV−vis spectroscopy in order to garner further mechanistic information on the formation of **1**. First, we note that the starting material, $(IMes)Fe(NTMS_2)_2$, is featureless in the visible range but possesses a broad absorbance in the near-UV region, starting at 350 nm and extending to the detector limit (275 nm) (Figure 3a, green band). In comparison, as described above, isolated product **1** exhibits two resonances centered at 316 and 362 nm that we assigned as LMCT bands (Figure 3a, black band). With this in mind, we monitored the growth and decay of absorption bands from the reaction of $(IMes)Fe(NTMS_2)_2$ under saturation kinetics with MsCl (100 equiv) in DCM over time. An initial absorption at 420 nm rapidly grows in within 10 min before gradually decaying to two new bands at 316 and 362 nm over the course of 3 h, consistent with the formation of **1** or **8**; however, these experimental conditions should favor the former and not the latter (Figure S38) We note that the initial band at 420 nm is analogous to that of **6** (Scheme 3, Figure S8) or the reported complex $Fe(NTMS_2)_2Cl(THF)$,[14] both of which are Fe^{III} species. The lack of a clean isosbestic

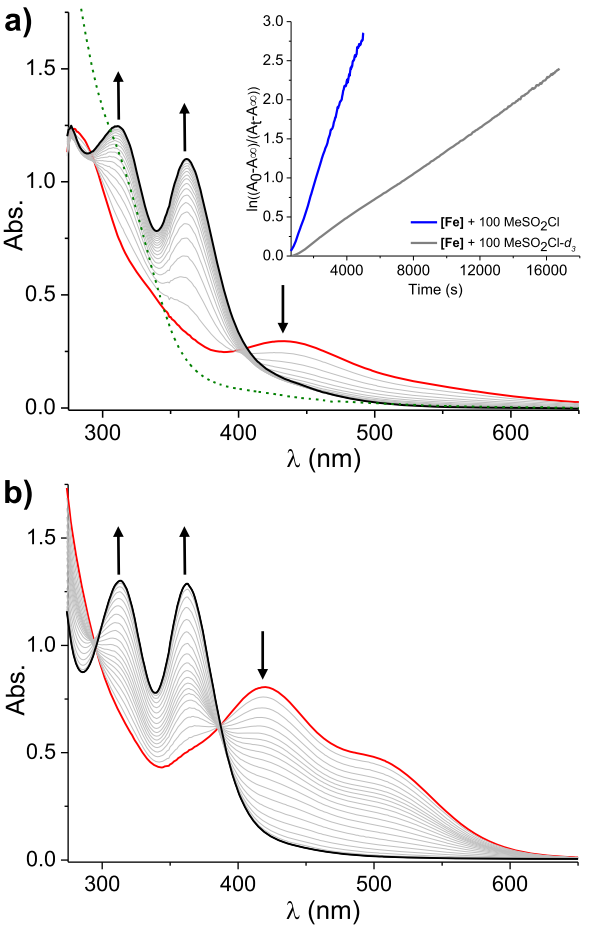

Figure 3. (a) UV−vis reaction of $(IMes)Fe(NTMS_2)_2$(green) with MsCl (100 equiv) showing the initial rapid growth of an Fe^{III} species (red), such as **6** (420 nm), followed by its decay to **1** (316 and 362 nm, black) over time (gray). Inset is the logarithmic plot of absorbance versus time for the decay of presumed **6** (420 nm) using MsCl (blue) and MsCl-d_3 (gray) revealing a primary kinetic isotope effect of 5.51 ± 0.01. (b) UV−vis reaction of **6** with MsCl (100 equiv) displaying the formation of **1** (black), but following a zero-order kinetic profile in **6**.

DOI: 10.1021/acs.organomet.9b00674
Organometallics XXXX, XXX, XXX−XXX

Scheme 5. Proposed General Mechanism for the Observed, Sterically Driven C−C versus C−Cl Bond-Forming Chemistry Starting from (IMes)Fe(NTMS$_2$)$_2$ and Alkylsulfonyl Chlorides[a]

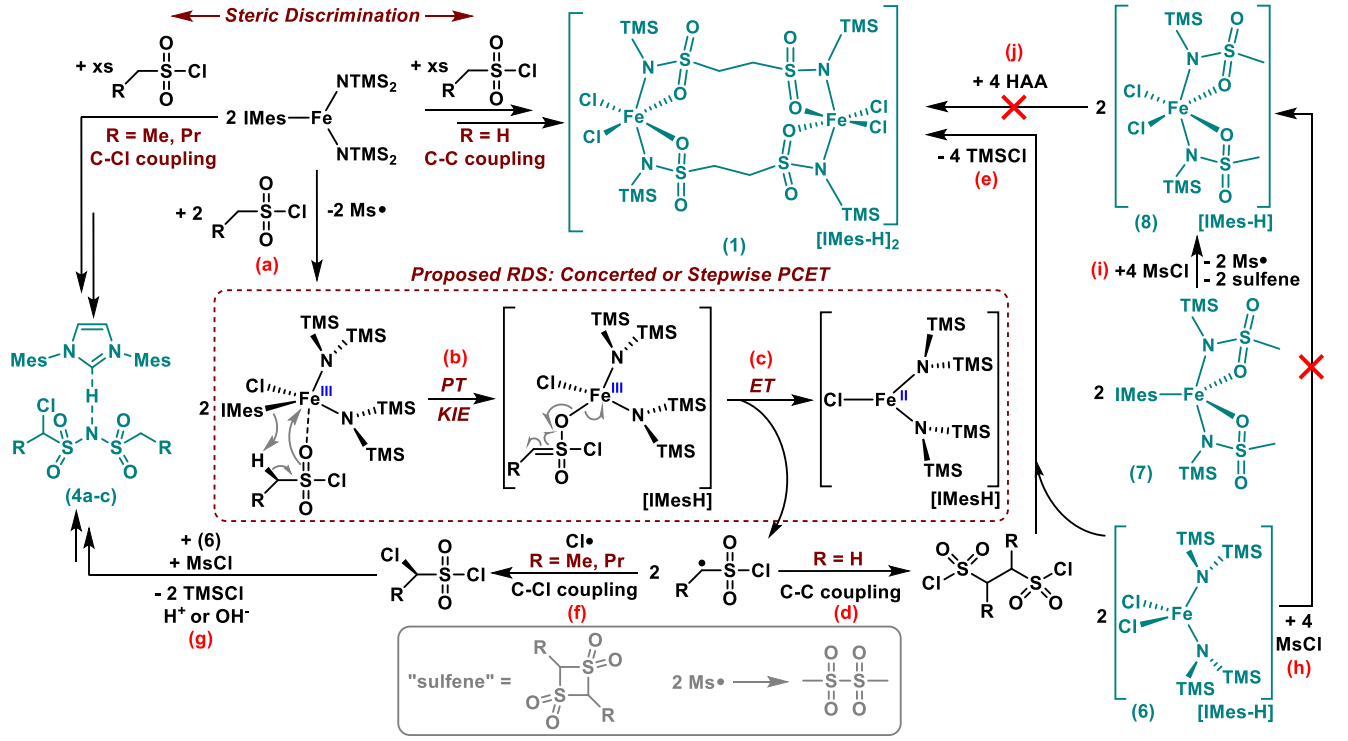

[a]A proposed RDS based on kinetic data and featuring a concerted or stepwise PCET reaction sequence is shown in the dashed box. Isolated compounds are drawn in teal and additional details are in gray. A supplemental mechanism accounting for the formation of **5a−c** and **9** is outlined in the Supporting Information.

point in this reaction is consistent with an expected multistep pathway involving numerous species. While the growth of **1** revealed no apparent reaction-order dependence, the conversion of **6** (or related Fe^{III} species) to **1** underwent pseudo-first-order decay. Furthermore, in monitoring the decay band at 420 nm, a primary kinetic isotope effect (KIE) of 5.51 ± 0.01 was found using deuterium-labeled MsCl-d_3 (Figure 3a, inset).[19]

To further probe the possible intermediacy of **6**, we separately subjected it to MsCl (100 equiv) in DCM and monitored its decay. While analogous decay features producing **1** were again observed, zero-order reaction kinetics were operational here (Figure 3b). However, we note that **6** contains protonated [IMesH]$^+$ in contrast to (IMes)Fe(NTMS$_2$)$_2$ which is known to contain free IMes in equilibrium.[11] Thus, introducing 3 equiv of IMes to the reaction mixture of **6** + MsCl (100 equiv) indeed reintroduced first-order kinetics throughout the reaction process. We were able to extract a pseudo-first-order rate constant of k' = 3.793 × 10^{-3} M^{-1} s^{-1} by independently varying the concentration of MsCl (Figures S14 and S15). To confirm that **1** and not the "half-piece" **8** (Scheme 3) is formed from the reaction of **6** with MsCl (2 equiv) (Scheme 5 path h), protonolysis of the reaction mixture with MeOH and subsequent analysis by ESI-MS revealed major peaks corresponding to the free ligand **2**, with no sign of the uncoupled fragment, MsNH(TMS) (Figure S40). Last, we investigated the reaction outcome in the absence of any IMes by synthesizing the previously reported Fe^{III} compound, [Et$_4$N][Cl$_2$Fe(NTMS$_2$)$_2$] (**10**).[20] We found that treatment of this complex with 2 equiv of MsCl resulted in a switch in product distribution, this time favoring the α-chlorinated product, **4a** (Scheme 6), and disfavoring the C(sp^3)−C(sp^3) coupled product (**2**), as observed by ESI-MS

Scheme 6. Reaction of 10 with MsCl (2 equiv) Leads to Switch in Product Distribution with α-Chlorination Product 4a Being Favored over C(sp^3)−C(sp^3) Product 3a

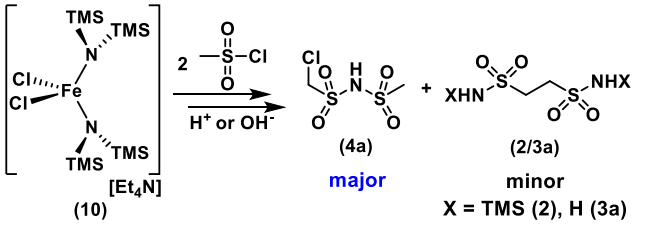

following protonolysis in MeOH (Figure S42). Together, these results highlight the importance of IMes in both the rate-determining step (RDS) and in controlling the chemoselectivity of this reaction.

We note that the Fe^{II} compound (**7**) (Scheme 3) is an unlikely intermediate given that initial TMSCl elimination to produce **7** from (IMes)Fe(NTMS$_2$)$_2$, followed by its oxidation to **8** or **1** would preclude the appearance of **6** (or a similar Fe^{III} species) in the UV−vis spectra (Figure 3). Furthermore, we found that the reaction of **7** with MsCl (2 equiv) yields **8**, not **1**, as determined by single-crystal XRD studies (Scheme 5path i). In parallel, ESI-MS analysis in negative-ion mode of the crude reaction mixture does not yield peaks for free ligand **2**. Last, we note that "half-piece" **8** is an unlikely intermediate given our unsuccessful attempts at H atom abstraction (HAA) to yield **1** following radical recombination (Scheme 5path j,

DOI: 10.1021/acs.organomet.9b00674
Organometallics XXXX, XXX, XXX−XXX

Figure S46). Together, these data support a reaction pathway involving initial fast oxidation of Fe^{II} to Fe^{III}, yielding intermediate **6** or a similar Fe^{III} species, followed by a rate-determining C−H functionalization step dependent on IMes and MsCl.

Combining the experimental data above and focusing first on the MsCl reaction with $(IMes)Fe(NTMS_2)_2$ (R = H, Scheme 5), we propose a general reaction mechanism involving the initial oxidation of $(IMes)Fe(NTMS_2)_2$ with MsCl resulting in the formation of an Fe^{III} species consistent with the observed absorption at 420 nm in the UV−vis spectrum (Scheme 5, path a, Figure 3a). Following this, a proposed RDS (Scheme 5, paths b + c (box)) dependent on both MsCl and IMes, and consistent with the observed KIE (Figure 3a), may involve a concerted or stepwise proton-coupled electron transfer (PCET) reaction resulting in C−H bond activation and the generation of the methylsulfonyl chloride radical which can rapidly dimerize to $ClSO_2CH_2CH_2SO_2Cl$ through $C(sp^3)-C(sp^3)$ bond formation (Scheme 5, path d). Finally, the reaction of this with either **6** or the proposed Fe^{II} intermediate $[IMesH][ClFe(NTMS_2)_2]$ (Scheme 5, path e) through TMSCl elimination (followed by oxidation for the latter) would lead to the final major product, **1**. On the basis of our experimental observations, this mechanism appears to be sterically driven. With the larger alkylsulfonyl chlorides, a competing reaction involving chlorination of the alkylsulfonyl chloride radical intermediate may result in the formation of products **4b,c** through a multistep pathway and following hydrolysis (Scheme 5, paths f and g). Last, the reactions described previously for compounds **6**−**8** are also described in Scheme 5 (paths h−j), whereas those outlining the formation of the minor products **5a**−**c** and **9** are described in section S10 of the Supporting Information.

CONCLUSIONS

To conclude, oxidative C−H functionalization of MsCl using an iron-carbene complex results in a new $C(sp^3)-C(sp^3)$ coupled product, **1**. Although heavier alkylsulfonyl chloride substrates similarly result in this type of coupling sequence, a reduction in chemoselectivity for C−C bond formation in favor of C−Cl and C−S bond formation is evidenced using the larger alkylsulfonyl chlorides. This work has demonstrated a potentially new avenue to generating $C(sp^3)-C(sp^3)$ bonds that may be used to build up complex molecular frameworks bearing bis(sulfonamide) functional groups.

ASSOCIATED CONTENT

Supporting Information

The Supporting Information is available free of charge at https://pubs.acs.org/doi/10.1021/acs.organomet.9b00674.

Materials and physical methods, synthesis, and supplemental figures (PDF)

Accession Codes

CCDC 1954777−1954786 contain the supplementary crystallographic data for this paper. These data can be obtained free of charge via www.ccdc.cam.ac.uk/data_request/cif, or by emailing data_request@ccdc.cam.ac.uk, or by contacting The Cambridge Crystallographic Data Centre, 12 Union Road, Cambridge CB2 1EZ, UK; fax: +44 1223 336033.

AUTHOR INFORMATION

Corresponding Author

*E-mail: menard@chem.ucsb.edu.

ORCID

Gabriel Ménard: 0000-0002-2801-0863

Notes

The authors declare no competing financial interest.

ACKNOWLEDGMENTS

We thank the National Science Foundation (CHE-1900651), the US-Israel Binational Science Foundation (#2016241), the ACS Petroleum Research Fund (#58693-DNI3), and the University of California, Santa Barbara, for financial support.

REFERENCES

(1) Coulston, G. W.; Bare, S. R.; Kung, H.; Birkeland, K.; Bethke, G. K.; Harlow, R.; Herron, N.; Lee, P. L. The Kinetic Significance of V5+ in n-Butane Oxidation Catalyzed by Vanadium Phosphates. *Science* **1997**, *275*, 191−193.

(2) Zhanglin, Y.; Forissier, M.; Sneeden, R. P.; Vedrine, J. C.; Volta, J. C. On the Mechanism of n-Butane Oxidation to Maleic Anhydride on VPO Catalysts: I. A Kinetics Study on a VPO Catalyst as Compared to VPO Reference Phases. *J. Catal.* **1994**, *145*, 256−266.

(3) Centi, G.; Trifiro, F.; Ebner, J. R.; Franchetti, V. M. Mechanistic aspects of maleic anhydride synthesis from C4 hydrocarbons over phosphorus vanadium oxide. *Chem. Rev.* **1988**, *88*, 55−80.

(4) Cheng, M.-J.; Goddard, W. A. The Critical Role of Phosphate in Vanadium Phosphate Oxide for the Catalytic Activation and Functionalization of n-Butane to Maleic Anhydride. *J. Am. Chem. Soc.* **2013**, *135*, 4600−4603.

(5) Cheng, M.-J.; Fu, R.; Goddard, W. A., III Design and validation of non-metal oxo complexes for C-H activation. *Chem. Commun.* **2014**, *50*, 1748−1750.

(6) Cheng, M.-J.; Goddard, W. A.; Fu, R. The Reduction-Coupled Oxo Activation (ROA) Mechanism Responsible for the Catalytic Selective Activation and Functionalization of n-Butane to Maleic Anhydride by Vanadium Phosphate Oxide. *Top. Catal.* **2014**, *57*, 1171−1187.

(7) Carroll, T. G.; Garwick, R.; Telser, J.; Wu, G.; Ménard, G. Synthesis, Characterization, and Electrochemical Analyses of Vanadocene Tetrametaphosphate and Phosphinate Derivatives. *Organometallics* **2018**, *37*, 848−854.

(8) Carroll, T. G.; Garwick, R.; Wu, G.; Ménard, G. A Mono-, Di-, and Trivanadocene Phosphorus Oxide Series: Synthesis, Magnetism, and Chemical/Electrochemical Properties. *Inorg. Chem.* **2018**, *57*, 11543−11551.

(9) Carroll, T. G.; Hunt, C.; Garwick, R.; Wu, G.; Dobrovetsky, R.; Ménard, G. An untethered C3v-symmetric triarylphosphine oxide locked by intermolecular hydrogen bonding. *Chem. Commun.* **2019**, *55*, 3761−3764.

(10) Chu, J.; Carroll, T. G.; Wu, G.; Telser, J.; Dobrovetsky, R.; Ménard, G. Probing Hydrogen Atom Transfer at a Phosphorus(V) Oxide Bond Using a "Bulky Hydrogen Atom" Surrogate: Analogies to PCET. *J. Am. Chem. Soc.* **2018**, *140*, 15375−15383.

(11) Layfield, R. A.; McDouall, J. J. W.; Scheer, M.; Schwarzmaier, C.; Tuna, F. Structure and bonding in three-coordinate N-heterocyclic carbene adducts of iron(ii) bis(trimethylsilyl)amide. *Chem. Commun.* **2011**, *47*, 10623−10625.

(12) Allen, F. H.; Kennard, O.; Watson, D. G.; Brammer, L.; Orpen, A. G.; Taylor, R. Tables of bond lengths determined by X-ray and neutron diffraction. Part 1. Bond lengths in organic compounds. *J. Chem. Soc., Perkin Trans. 2* **1987**, *2*, S1−S19.

(13) Gütlich, P. Fifty Years of Mössbauer Spectroscopy in Solid State Research − Remarkable Achievements, Future Perspectives. *Z. Anorg. Allg. Chem.* **2012**, *638*, 15−43.

DOI: 10.1021/acs.organomet.9b00674
Organometallics XXXX, XXX, XXX−XXX

444 (14) Duncan, J. S.; Nazif, T. M.; Verma, A. K.; Lee, S. C. Iron-
445 Arylimide Clusters [Fem(NAr)nCl4]2- (m, n = 2, 2; 3, 4; 4, 4) from a
446 Ferric Amide Precursor: Synthesis, Characterization, and Comparison
447 to Fe-S Chemistry. *Inorg. Chem.* **2003**, *42*, 1211−1224.
448 (15) Roy, A. K. Novel synthesis of sulfonimidoyl halides and
449 sulfonimidates from N-silylated sulfonamides and dihalophosphor-
450 anes. *J. Am. Chem. Soc.* **1993**, *115*, 2598−2603.
451 (16) Hanefeld, W.; Spangenberg, B. Ein inverser Aminangriff an
452 Sulfen unter Bildung neuer Ammonio-sulfobetaine. *Chem. Ber.* **1988**,
453 *121*, 1147−1150.
454 (17) Broere, D. L. J.; Mercado, B. Q.; Holland, P. L. Selective
455 Conversion of CO2 into Isocyanate by Low-Coordinate Iron
456 Complexes. *Angew. Chem., Int. Ed.* **2018**, *57*, 6507−6511.
457 (18) Aldeva, V.; Gezahegn, S.; Panahi, B.; Shuoprasad, M.; Ward, J.;
458 Foucher, D. A.; Gossage, R. A.; McWilliams, A. R. Synthesis,
459 Characterization, and Theoretical Analysis of Soluble Poly-
460 (oxothiazenes): The Ambient Temperature Lewis Acid Catalyzed in
461 Situ Polymerization of N-Silylsulfonimidoyl Chlorides. *Macromolecules*
462 **2013**, *46*, 2562−2568.
463 (19) Westheimer, F. H. The Magnitude of the Primary Kinetic
464 Isotope Effect for Compounds of Hydrogen and Deuterium. *Chem.*
465 *Rev.* **1961**, *61*, 265−273.
466 (20) Duncan, J. S.; Zdilla, M. J.; Lee, S. C. Synthesis and Elaboration
467 of the Dinuclear Iron-Imide Cluster Core [Fe2(μ-NR)2]2+. *Inorg.*
468 *Chem.* **2007**, *46*, 1071−1080.

DOI: 10.1021/acs.organomet.9b00674
Organometallics XXXX, XXX, XXX−XXX